Light Curve Analysis of Eclipsing Binary Stars LX Leo, V345 UMa, and MU Leo

Lauren Hoffman
Vince Mazzola
Vayujeet Gokhale
Truman State University, 100 E. Normal Street, Kirksville, MO, 63501; gokhale@truman.edu

Received February 18, 2021; revised March 3, May 26, 2022; accepted May 31, 2022

Abstract We present light curve analysis of three eclipsing binary stars, LX Leo, V345 UMa, and MU Leo, using data collected at the 31-inch NURO telescope at Lowell Observatory in Flagstaff, Arizona, in three filters: Bessell B, V, and R. We generate truncated twelve-term Fourier fits for the light curves to: a) confirm that LX Leo and V354 UMa are W UMa type, and MU Leo is an Algol type eclipsing binary star system and, b) quantify the light curve asymmetries exhibited by each of these systems in each filter. The asymmetries in the light curves are quantified by calculating the difference in the heights of the primary and secondary maxima (ΔI), the "Light Curve Asymmetry" (LCA), and the "O'Connell Effect Ratio" (OER). Of the systems studied here, we find that V354 UMa has the most symmetric curve and LX Leo has the most asymmetric curve. We also find that for each object, generally, the asymmetries are more pronounced in the B-filter.

1. Introduction

For the past few years, undergraduate students at Truman State University (Kirksville, Missouri) have been involved in quantifying the asymmetries in the light curves of Eclipsing Binary (EB) stars (Gardner *et al.* 2015; Akiba *et al.* 2019; Hahs *et al.* 2020). In this paper, we extend these analyses to three additional EB systems: LX Leo (P = 0.235247 d), V345 UMa (P = 0.293825 d), and MU Leo (P = 0.388442 d). All three objects were selected from a list of eclipsing binaries published by Kreiner (2004).

Following Akiba *et al.* (2019), we quantify the asymmetries in the light curves by calculating three quantities using the Fourier fits: the difference in the heights of the primary and secondary maxima (ΔI, traditionally referred to as the "O'Connell Effect," O'Connell 1951), the Light Curve Asymmetry (LCA, McCartney 1999), and the O'Connell Effect Ratio (OER). Additionally, we use Fourier fitting of the light curves to classify these EB systems into Algol, β Lyrae, or W UMa type systems.

Photometric studies of LX Leo (Gürol *et al.* 2017) and V354 UMa (Michel *et al.* 2019) have already characterized these systems as W UMa type variables. Gürol *et al.* (2017) have noticed the asymmetry in the light curve and use this asymmetry to model the system with starspots. On the basis of their light curve solution, Gürol *et al.* (2017) conclude that LX Leo is a W UMa type system with a mass ratio q = 1.89 ± 0.02. Similarly, Michel *et al.* (2019) provide a photometric solution for V354 UMa and conclude that it is also a W UMa type system with a mass ratio q = 3.623 ± 0.040. They suggest that V354 UMa has an asymmetric light curve, suggesting the presence of either star spots or dark spots. Further, Michel *et al.* 2019) also suggest that this system exhibits a variable orbital period, implying conservative mass transfer from the less massive to the more massive component.

In this paper, we are interested in quantifying the asymmetries in the light curves in the aforementioned ways (McCartney 1999), as a first step towards understanding the origins of the asymmetries. Traditionally (see Gürol *et al.* 2017, Michel *et al.* 2019, for example), these asymmetries are attributed to either "starspots" (cooler regions on one or the other star) or to "hotspots" (usually associated with mass transfer in close binary systems). Due to lack of spectroscopic data, we do not attempt to model these systems, and hence are not in a position to comment on the efficacy of either of these models. We believe that even with access to spectroscopic data, a true model of these systems is elusive unless the systems are observed over a long timeline in order to model *changes* in the light curves of these objects. To overcome this limitation, in a forthcoming publication (Knote *et al.* 2022), we are analyzing uninterrupted data from the Kepler (Prša 2011) and Transiting Exoplanet Survey Satellite (TESS) missions (Ricker *et al.* 2015) to better constrain the system parameters and hence, determine the elusive origin of these asymmetries.

In the following section, we outline the data acquisition and data reduction methods we employed. Our results and analyses are presented in section 3, followed by a discussion section summarizing our results, conclusions, and plans for the future.

2. Observations

We obtained data on three eclipsing variable stars: LX Leo (P = 0.235247), MU Leo (NSVS 7504057) (P = 0.388442), and V354 UMa (P = 0.293825), using the 2k × 2k Loral NASACam CCD attached to the 31-inch National Undergraduate Research Observatory (NURO) telescope in Flagstaff, Arizona. The data were taken on UT dates 03/20/2020, 03/14/2020, and 03/18/2020, respectively. The filters used are Bessell BVR. The images taken were processed using bias subtraction and flat fielding by constructing a master bias and master flat image using the AstroImageJ software (AIJ, v3.2, Collins *et al.* 2017). Dark subtraction was not needed due to the nitrogen-cooled camera at NURO, thus making the dark current negligible.

Differential photometry was then performed on our target stars with suitable comparison and check stars when possible using the AIJ software. We used the radial profile display utility

Table 1. Target, comparison and check star coordinates comparison star B and V magnitudes used for data from the NURO telescope.

Star	*Name*	*R.A. (J2000)*	*Dec. (J2000)*	*V*	*B*
Target	LX Leo	09 50 27072	+20 43 05.34	—	—
Comparison	TYC 1417-387-1	09 50 47.29	+20 39 01.24	11.18	11.65
Check	TYC 1417-423-1	09 49 58.99	+20 42 11.83	12.19	13.08
Target	V354 UMa	13 35 38.40	+49 14 06.12	—	—
Comparison	TYC 3466-293-1	13 35 26.02	+49 08 1910	10.27	11.21
Check	TYC 3466-294-1	13 35 06.49	+49 17 51.68	11.80	12.21
Target	MU Leo	10 24 59.90	+24 30 51.56	—	—
Comparison	TYC 1969-496-1	10 24 53.53	+24 24 41.99	10.28	11.14

Table 2. Classification of systems based on Fourier coefficients.

Target	*Filter*	a_1	a_2	a_4	$a_2 (0.125 - a_2)$	*Classification*
LX Leo	B	0.0023 ± 0.0008	–0.2265 ± 0.0009	–0.0586 ± 0.0010	–0.0796 ± 0.0004	W UMa
	V	0.0003 ± 0.0007	–0.2211 ± 0.0008	–0.0590 ± 0.0008	–0.0765 ± 0.0004	W UMa
	R	–0.0036 ± 0.0006	–0.2155 ± 0.0006	–0.0600 ± 0.0007	–0.0734 ± 0.0003	W UMa
V354 UMa	B	0.0048 ± 0.0002	–0.0651 ± 0.0002	–0.0009 ± 0.0002	–0.01238 ± 0.00004	W UMa
	V	0.0057 ± 0.0002	–0.0617 ± 0.0002	–0.0011 ± 0.0002	–0.01151 ± 0.00004	W UMa
	R	0.0053 ± 0.0002	–0.0595 ± 0.0002	–0.0008 ± 0.0002	–0.01097 ± 0.00004	W UMa
MU Leo	B	0.0812 ± 0.0006	–0.1567 ± 0.0006	–0.0716 ± 0.0006	–0.0441 ± 0.0002	Algol
	V	0.0734 ± 0.0005	–0.1546 ± 0.0005	–0.0759 ± 0.0006	–0.0432 ± 0.0002	Algol
	R	0.0582 ± 0.0006	–0.1526 ± 0.0006	–0.0779 ± 0.0007	–0.0424 ± 0.0002	Algol

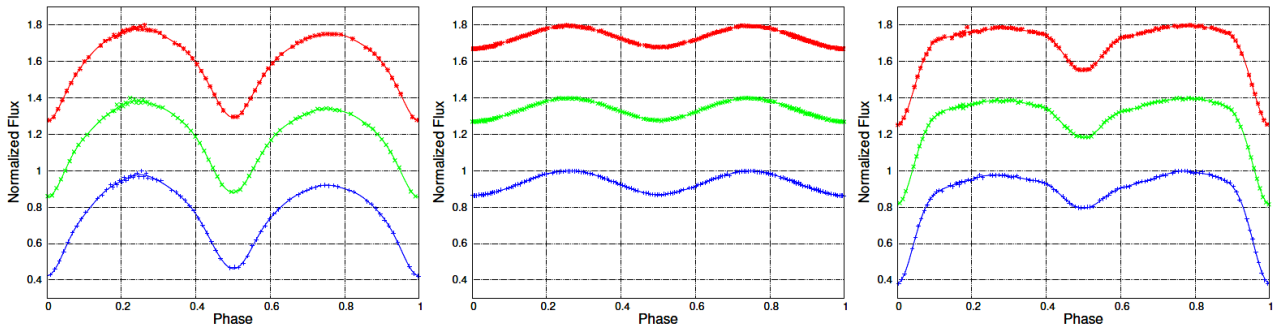

Figure 1. Normalized flux for LX Leo (left), V354 UMa (center), and MU Leo (right) in all three filters. The Fourier fits (continuous curves) are plotted along with the blue, green, and red curves corresponding to B, V, and R filters, respectively. The average error in the flux for each measurement is approximately 0.003 and 0.005 for LX Leo and V354 UMa, respectively, in all filters, and about 0.0002 for MU Leo in all filters. Error bars are not shown for the sake of clarity.

function in AIJ to determine the photometric aperture radius and the radii of the inner and outer annulus, using the method outlined in Collins *et al.* (2017) (see their Appendix A). To search for comparison and check stars, we used the SIMBAD Astronomical Database (Wenger *et al.* 2000) to find any stars in the image frame relatively close in brightness and size to our target star. We then used the cataloged B and V magnitudes of the comparison stars to determine the corresponding magnitudes of each of our target stars (Table 1). Instrumental magnitudes were used for the R-filter since the R magnitude was not listed. We also ensured that the comparison and check stars chosen showed no variability in each of the filters. All differential photometry data can be retrieved from the AAVSO International Database (Kafka 2021). These data are also available on request via email: gokhale@truman.edu and are available at http://gokhale.sites.truman.edu/asymmetries/.

3. Analysis

The analysis of the light curves in this paper closely follows the procedure outlined in Gardner *et al.* (2015), Akiba *et al.* (2019), and Hahs *et al.* (2020). We first phase-fold the time axis and ensure that the primary (deeper) eclipse always coincides with phase "0." Additionally, we calculate the normalized flux for each data point from the measured magnitudes obtained via differential photometry (Warner and Harris 2006) as:

$$I(\Phi)_{obs} = 10^{-0.4 \times (m(\Phi) - m(max))} \quad (1)$$

where m(Φ) is the magnitude at a certain phase Φ and m(max) is the maximum magnitude observed for the object. We perform Fourier fit analyses on the light curves of each object in each filter similar to Wilsey and Beaky (2009). A truncated twelve-term Fourier fit is given by

$$I(\Phi)_{fit} = a_0 + \sum_{n=1}^{12} (a_n \cos(2\pi n \Phi) + b_n \sin(2\pi n \Phi)) \quad (2)$$

where a_0, a_n, and b_n are the Fourier coefficients of the fit, and Φ is the phase (Hoffman *et al.* 2009). The light curves of the three objects in each filter along with their Fourier fits are presented in Figure 1.

3.1. Classification

Following Akiba *et al.* (2019), the Fourier coefficients and the associated errors are extracted from the Fourier fits generated using MATHEMATICA (Wolfram Research Co. 2019) and are tabulated in Table 2. The values of these coefficients are determined by the shape of the light curves, and hence are a quantitative measure of the geometry of the eclipsing binary (Ruciński 1973, 1993, 1997). In particular, the condition $a_4 < a_2 (0.125 - a_2)$ implies that the system is a detached system and is classified as an Algol-type system (see Akiba *et al.* 2019) for details). If this condition is not met, and additionally if $|a_1| < 0.05$, then the system is classified as a W UMa type system; otherwise it is classified as a β Lyrae type system.

For the three systems under consideration, in all three filters, the results from the Fourier coefficient method are consistent with those from qualitative visual inspection: LX Leo and V354 UMa are confirmed to be W UMa type systems, while MU Leo is of the Algol-type.

3.2. Quantifying the asymmetries in the light curves

We quantify the asymmetries in several different ways:

1. For each object, in each filter, we determine the difference in the normalized flux near the primary and secondary maxima from the data (ΔI_{ave}) and from the fit (ΔI_{fit}). Additionally, we determine $|2b_1|$ from the Fourier coefficient b_1, since this term represents the half-amplitude of the sine wave of the Fourier fit and is thus a measure of the difference between the primary and secondary maxima (Wilsey and Beaky 2009). These values are tabulated in Table 3. It is clear that V354 UMa has the smallest, if any, asymmetry in its light curve, followed by MU Leo, for which ΔI is negative. LX Leo has the greatest amount of asymmetry. Generally, ΔI is greatest in the B filter, which is consistent with the results obtained by Akiba *et al.* (2019).

2. For each object, in each filter, we determine the O'Connell Effect ratio (OER) and the Light Curve Asymmetry (LCA, McCartney 1999) using:

$$OER = \frac{\int_{0.0}^{0.5} (I(\Phi)_{fit} - I(0.0)_{fit}) d\Phi}{\int_{0.5}^{1.0} (I(\Phi)_{fit} - I(0.0)_{fit}) d\Phi} \quad (3)$$

and,

$$LCA = \sqrt{\int_{0.0}^{0.5} \frac{(I(\Phi)_{fit} - I(1.0 - \Phi)_{fit})^2}{I(\Phi)^2_{fit}} d\Phi} \quad (5)$$

Table 3. Quantifying the O'Connell Effect in terms of difference in maxima (see section 3.2 for details).

Target	*Filter*	$\|2b_1\|$	*ΔI (Fourier)*	*ΔI (Average)*
LX Leo	B	0.043 ± 0.001	0.058 ± 0.007	0.053 ± 0.001
	V	0.035 ± 0.001	0.044 ± 0.006	0.040 ± 0.001
	R	0.023 ± 0.001	0.033 ± 0.005	0.029 ± 0.001
V0354 UMa	B	0.0020 ± 0.0002	0.000 ± 0.002	0.000 ± 0.002
	V	0.0002 ± 0.0003	0.000 ± 0.002	0.000 ± 0.003
	R	0.0016 ± 0.0003	–0.001 ± 0.002	0.000 ± 0.002
MU Leo	B	0.018 ± 0.001	–0.022 ± 0.005	–0.0201 ± 0.0001
	V	0.011 ± 0.001	–0.012 ± 0.004	–0.0123 ± 0.0001
	R	0.013 ± 0.001	–0.001 ± 0.005	–0.0120 ± 0.0001

Table 4. Quantifying the O'Connell Effect in terms of OER and LCA (see section 3.2 for the definitions of the OER and LCA).

Target	*Filter*	*OER*	*LCA*
LX Leo	B	1.08 ± 0.02	0.025 ± 0.003
	V	1.07 ± 0.02	0.020 ± 0.003
	R	1.05 ± 0.02	0.014 ± 0.002
V0354 UMa	B	1.02 ± 0.02	0.003 ± 0.001
	V	1.00 ± 0.03	0.002 ± 0.001
	R	1.02 ± 0.03	0.003 ± 0.001
MU Leo	B	0.98 ± 0.01	0.021 ± 0.002
	V	0.99 ± 0.01	0.013 ± 0.002
	R	0.99 ± 0.01	0.015 ± 0.002

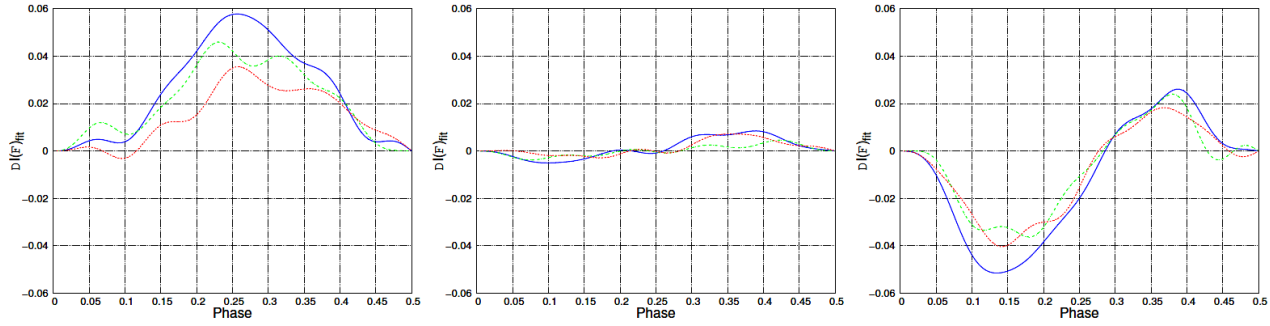

Figure 2. Difference in normalized flux between the two halves of the light curves, in the B (blue solid curve), V (green dashed), and R (red dotted) filters for LX Leo (left plot), V354 UMa (middle), and MU Leo (right). In the absence of any asymmetry, the two curves should coincide, and the solid blue curve in the bottom panel would be a flat line at "0."

The asymmetry reflected by the OER and LCA values (Table 4) are consistent with the ΔI values from Table 3. We note that V354 UMa has a very symmetric light curve, while LX Leo has a significant asymmetry as quantified by both the OER and LCA. Interestingly, MU Leo has a low OER in each filter, though the LCA is significant (see below). We do not observe any obvious trend in the amount of asymmetry as a function of filter, though generally, the OER and LCA are the greatest in the B-filter which is consistent with the results obtained by Gardner *et al.* (2015), Akiba *et al.* (2019), and Hahs *et al.* 2020). Of course, a much larger sample is necessary to derive any reliable conclusions regarding the filter-dependance of light curve asymmetries in EB light curves.

3. Additionally, we superpose the two halves of each of the light curves to generate "half-phase plots" to visually demonstrate the asymmetries. We do this by "mirroring" the light curve about the phase 0.5, and in Figure 2 we plot the difference between the flux at equivalent phases in the light curve (for example, phases $\Phi = 0.2$ and $\Phi = 0.8$). Consequently, this plot helps to indicate the phases around which the curve is most asymmetric, and where, for example, star spots may be located under the starpot model to explain these asymmetries. It is again clear that V354 UMa has a very symmetric light curve. It is interesting to note that for LX Leo, in all filters, the primary half of the light curve has a greater flux than the secondary half ($\Delta I(\Phi)_{fit} > 0$). On the other hand, in MU Leo (and to some extent in V354 UMa), the contribution to the flux varies with phase - starting off with greater flux on the secondary side ($\Delta I(\Phi)_{fit} > 0$ between phases 0.0–0.3, or equivalently, phases 0.7–1.0) and moving toward higher contributions from the primary side ($\Delta I(\Phi)_{fit} < 0$ between phases 0.3–0.5 or phases 0.5–0.7). Thus, even though MU Leo has an OER ≈ 1, the "half-phase" plot (Figure 2) demonstrates that there is still significant asymmetry in its light curve. The "half-phase" plots are a visual demonstration of the LCA parameter, and the example of MU Leo demonstrates the advantages of quantifying the asymmetries in different ways.

4. Discussion

We have quantified the asymmetries in three short period eclipsing binary systems: LX Leo (P = 0.235247 d), V345 UMa (P = 0.293825 d), and MU Leo (P = 0.388442 d). Of these, V354 UMa exhibits the most symmetric light curve, while LX Leo is the most asymmetric. We have confirmed that LX Leo and V354 UMa are W UMa-type systems, while MU Leo is an Algol-type system. For LX Leo, the asymmetry is greatest around phase 0.25, while for MU Leo, it is greatest near phase 0.15. By visual inspection, it is clear that LX Leo has a positive O'Connell Effect (primary maxima is higher than secondary maxima) in all three filters. This bears out in the positive values of ΔI and the fact that OER > 1. For MU Leo, ΔI is negative in all filters, which is consistent with the shape of the light curve for MU Leo (Figure 1). Note also, for MU Leo, the OER $\lesssim 1$ in all three filters, showing there is slightly less flux in the primary half of the light curve than the secondary half, but overall, there is almost equal flux in the two halves. Despite this, the LCA is significant, and clear asymmetries are evident in the "half-phase plots" in Figure 2. In all three filters, the values of ΔI for V354 UMa are essentially zero implying a very small O'Connell effect. Similarly, the OER is quite small for V354 UMa, and the LCA is almost an order of magnitude smaller than the other two objects, implying an very symmetric curve for V354 UMa.

We do not discern any obvious correlation between the type of filter used and any of the asymmetry parameters we have discussed, except to note that the asymmetries seem to be more pronounced in the B-filter.

As mentioned earlier, we are currently working on several EBs from the Kepler and TESS catalogs (Knote *et al.* 2022). Our goal is to extend the work presented here to hundreds of objects, and study the time evolution of the asymmetries over several hundreds and thousands of orbital cycles. We hope to discern patterns in the changes in the asymmetries by addressing questions such as: *What are the timescales over which the asymmetries change? Are there differences in the asymmetries in over-contact, semi-detached, and detached systems? Why do the asymmetries in certain systems remain very steady, while in other systems the asymmetries vary significantly over relatively short timescales?*, and so on.

5. Acknowledgements

We have made extensive use of the tools available on the AAVSO website, in particular the VSP (Variable Star Plotter) tool to generate star charts. In addition, we have used the SIMBAD database, operated at CDS, Strasbourg, France, and NASA's Astrophysics Data System. We are thankful for the support provided by the Office of Student Research at Truman State University and the Missouri Space Grant Consortium.

References

Akiba, T., Neugarten, A., Ortmann, C., and Gokhale, V. 2019, *J. Amer. Assoc. Var. Star Obs.*, **47**, 186.

Collins, K. A., Kielkopf, J. F., Stassun, K. G., and Hessman, F. V. 2017, *Astron. J.*, **153**, 77.

Gardner, T., Hahs, G., and Gokhale, V. 2015, *J. Amer. Assoc. Var. Star Obs.*, **43**, 186.

Gürol, B., Michel, R., and Gonzalez, C. 2017, *Rev. Mex. Astron. Astrofis.*, **53**, 179.

Hahs, G., Ortmann, C., and Gokhale, V. 2020, J. *Amer. Assoc. Var. Star Obs.*, **57**, 48.

Hoffman, D. I., Harrison, T. E., and McNamara, B. J. 2009, *Astron. J.*, **138**, 466.

Kafka, S. 2021, Observations from the AAVSO International Database (https://www.aavso.org/data-download).

Knote, M. K., *et al.* 2022, *Astrophys. J., Suppl. Ser.*, accepted (https://arxiv.org/abs/2206.04142).

Kreiner, J. M. 2004, *Acta Astron.*, **54**, 207.

McCartney, S. A. 1999, Ph.D. dissertation, University of Oklahoma.

Michel, R., Xia, Q.-Q., and Higuera, J. 2019, *Res. Astron. Astrophys.*, **19**, 99 (DOI: 10.1088/1674-4527/19/7/99).

O'Connell, D. J. K. 1951, *Publ. Riverview Coll. Obs.*, **2**, 85.

Prša, A., *et al.* 2011, *Astron. J.*, **141**, 83.

Ricker G. R., *et al.* 2015, *J. Astron. Telesc. Instrum. Syst.*, **1**, 014003.
Ruciński, S. M. 1973, *Acta Astron.*, **23**, 79.
Ruciński, S. M. 1993, *Publ. Astron. Soc. Pacific*, **105**, 1433.
Ruciński, S. M. 1997, *Astron. J.*, **113**, 407.
Warner, B. D., and Harris, A. W. 2006, *A Practical Guide to Lightcurve Photometry and Analysis*, Springer, New York.
Wenger, M., *et al.* 2000, *Astron. Astrophys., Suppl. Ser.*, **143**, 9 (DOI: 10.1051/aas:2000332).
Wilsey, N. J., and Beaky M. M. 2009, in *The Society for Astronomical Sciences 28th Annual Symposium on Telescope Science*, Society for Astronomical Sciences, Rancho Cucamonga, CA, 107.
Wolfram Research Co. 2019, How to Fit Models with Measurement Errors (https://reference.wolfram.com/language/howto/FitModelsWithMeasurementErrors).